A SYMMETRIC DISCRETIZATION OF THE PERFECTLY MATCHED LAYER FOR THE 2D HELMHOLTZ EQUATION

HYUNSEO PARK[1], HYEONJUN SONG[2], YOONSEO PARK[3] and CHANGSOO SHIN[2]

[1]*Department of Mechanical and Aerospace Engineering, Seoul National University, South Korea. sseleman@snu.ac.kr*
[2]*Department of Energy Systems Engineering, Seoul National University, South Korea. weoever@gmail.com; cssmodel@snu.ac.kr*
[3]*Computational Science and Technology Program, Seoul National University, South Korea. pp22ppgo@naver.com*

(Received April 8, 2017; revised version accepted September 18, 2017)

ABSTRACT

Park, H., Song, H., Park, Y. and Shin, C., 2017. *Journal of Seismic Exploration*, 26: 541-560.

A symmetric discretization of the Perfectly Matched Layer (PML) for the 2D Helmholtz equation is introduced. The PML is an efficient method to suppress spurious reflections at the boundaries of the computational domain, so that the Sommerfeld radiation condition in unbounded medium is effectively achieved. The PML can be formulated in the symmetric form, which has not been used with dispersion-minimizing finite difference methods in the exploration geophysics community. We suggest a simple symmetrization of the discretized matrix that can be used with a dispersion-minimizing method. The symmetric discretization of the PML enables us to utilize the LDLT (LDL^T) decomposition with the Bunch-Kaufman pivoting, which considerably reduces not only the number of arithmetic operations but also storage requirement for numerical factorization of a sparse matrix, compared to the LU decomposition. Some numerical experiments are shown to demonstrate the efficiency of the suggested scheme.

KEY WORDS: acoustic wave, Helmholtz equation, symmetric matrix, finite difference, absorbing boundary, numerical dispersion minimization.

0963-0651/17/$5.00

INTRODUCTION

The acoustic wave equation has been widely used for many engineering problems and also geophysical applications such as reverse time migration (Baysal et al., 1983) and full waveform inversion (Tarantola, 1984). Full waveform inversion has been performed by the time domain acoustic wave equation (Tarantola, 1984) or the Helmholtz equation (Shin, 1988; Pratt et al., 1998), which expresses time-harmonic wavefields of acoustic, elastic and electromagnetic wave phenomena in the frequency domain. The computational costs in such applications are typically large. Therefore, an efficient numerical method is required.

Properly suppressing boundary reflections is one of the efficiency factors. It gives a smaller size of the computational domain and the subsequent reduction of the computational costs. The reflectionless boundary condition can be effectively mimicked by using the Perfectly Matched Layer (PML) technique (Bérenger, 1994, 2007). The PML has a great absorbing ability without reflections at the boundaries regardless of incidence angles (except for glancing angles, actually), therefore, the size of the truncated domain is reduced.

The PML can be formulated equivalently in either symmetric or nonsymmetric form, and the numerical factorization cost of the discretized matrix may be different depending on the symmetricity of the PML. If the PML is applied on the conventional second order finite difference scheme, then the PML can be easily formulated in the symmetric form, which enables us to discretize a Helmholtz problem as a symmetric indefinite system. It can enjoy the LDLT decomposition with the Bunch-Kaufman pivoting (Bunch and Kaufman, 1977), which reduces computational time and memory cost compared to the LU decomposition. However, in the exploration geophysics community, only the nonsymmetric PML has been used for most dispersion-minimizing methods (Hustedt et al., 2004; Operto et al., 2007; Chen, 2014). As a result, the general sparse LU decomposition has been employed to solve the nonsymmetric matrix.

When dispersion-minimizing methods are employed, the resultant discretized matrix may not be symmetric even if the form of the PML is symmetric. We will show how to construct a symmetric matrix incorporating the dispersion-minimizing property and the PML together.

METHODS

Symmetric PML

The Helmholtz equation, or second order acoustic wave equation in the frequency domain is expressed as

$$-\left(\frac{\omega^2}{v^2}\right)p - \partial_x^2 p - \partial_z^2 p = f \quad , \tag{1}$$

where v is the local acoustic wave speed, ω is the angular frequency, p is the pressure wavefield, and f is the source or forcing function of the system. The spatial support of the source function f in many geophysical applications is typically a Dirac delta function, which represents a seismic point source like an air-gun array. Appropriate boundary conditions such as free surface condition also should be imposed. In the following derivation of the symmetric PML equation, the source f will be omitted without loss of generality because sources are located only in non-PML region, where the PML equation reduces to the ordinary Helmholtz equation [eq. (1)].

The PML can be implemented easily in the frequency domain by using complex coordinate stretching interpretation (Chew and Weedon, 1994; Sacks et al., 1995). Coordinate stretching by a complex-valued factor introduces a damping effect acting only on wave components whose propagation direction is parallel to each orthogonal coordinate axis. Each coordinate is stretched by a factor of $s_x(x) = 1 + d_x(x)/(\pm i\omega)$ or $s_z(z) = 1 + d_z(z)/(\pm i\omega)$. The sign of $i\omega$ depends on the Fourier transform convention. Damping strength $d_x(x)$ and $d_z(z)$ are zero in non-PML region and gradually increase as the depth deepens into the PML region. The profile of damping strength may vary like quadratic or cubic polynomials, but more complicated profiles can also be used. The non-uniform coordinate scaling $(x, z) \rightarrow (s_x x, s_z z)$ can be systematically injected to eq. (1) by applying a simple transformation rule

$$\partial_x \rightarrow \left(\frac{1}{s_x}\right)\partial_x, \qquad \partial_z \rightarrow \left(\frac{1}{s_z}\right)\partial_z \ . \tag{2}$$

After applying the transformation rule and replacing ω/v with a wavenumber k to simplify the notation, eq. (1) is transformed to

$$-k^2 p - \left(\frac{1}{s_x}\right)\partial_x \left(\frac{1}{s_x}\right)\partial_x p - \left(\frac{1}{s_z}\right)\partial_z \left(\frac{1}{s_z}\right)\partial_z p = 0. \tag{3}$$

As mentioned above, a source f is excluded in eq. (3). Eq. (3) is a popular PML form used in the exploration geophysics communities, where some dispersion-minimizing finite difference methods (Hustedt et al., 2004; Operto et al., 2007; Chen, 2014) rely on eq. (3). The form of linear operator in eq. (3) is nonsymmetric even prior to discretization. Multiplying eq. (3) by $s_x s_z$, we easily obtain a symmetrized version of acoustic wave equation with PML coefficients s_x and s_z

$$-k^2 s_x s_z p - \partial_x \left(\frac{s_z}{s_x}\right)\partial_x p - \partial_z \left(\frac{s_x}{s_z}\right)\partial_z p = 0 \, . \tag{4}$$

The symmetrized equation [eq. (4)] was introduced at an early development stage of the PML (Sacks et al., 1995; Turkel and Yefet, 1998), but it has not been widely recognized in the exploration geophysics communities. Although the operator of eq. (4) is not Hermitian/self-adjoint ($A^H = A$; the superscript H means the conjugate transpose.), it is symmetric with complex coefficients ($A^T = A$; the superscript T means the transpose.). Thanks to the symmetry, computational efficiency directly comes from replacement of the sparse LU decomposition with the sparse LDLT decomposition with the Bunch-Kaufman 2 by 2 diagonal pivoting, which is able to factorize a complex symmetric indefinite matrix (Bunch and Kaufman, 1977).

Conventional Discretization with the Symmetric PML

Our starting point of the following discretization is eq. (4), whose linear operator has a complex-valued symmetric indefinite form. Discretization of the linear operator also results in a complex symmetric indefinite matrix, so that the sparse LDLT decomposition with the Bunch-Kaufman pivoting can be utilized.

We first define finite difference operators δ_x and δ_z for first derivatives in each coordinate direction

$$\begin{aligned} \delta_x p_{0,0} &= (p_{1/2,0} - p_{-1/2,0})/\Delta x, \\ \delta_z p_{0,0} &= (p_{0,1/2} - p_{0,-1/2})/\Delta z. \end{aligned} \tag{5}$$

Grid intervals are denoted by Δx and Δz. Subscripts denote positions of nodal points relative to some reference coordinates (x_0, z_0) on discrete grids, for example, $p_{0,0} = p(x_0, z_0)$ and $p_{1,0} = p(x_0 + \Delta x, z_0)$, etc. Half-integer index like $p_{1/2,0} = p(x_0 + \Delta x/2, z_0)$ indicates that it is defined at a staggered position. By one more successive application of the finite difference operators [eq. (5)], we may also form second derivatives

$$\begin{aligned} \delta_x^2 p_{0,0} &= (p_{1,0} - 2p_{0,0} + p_{-1,0})/\Delta x^2, \\ \delta_z^2 p_{0,0} &= (p_{0,1} - 2p_{0,0} + p_{0,-1})/\Delta z^2. \end{aligned} \tag{6}$$

If we follow a conventional 5-point stencil discretization of eq. (4) using the finite difference operators, then the discretized equation becomes

$$-(k^2 s_x s_z)|_{0,0} p_{0,0} - \delta_x (s_z/s_x)\delta_x p_{0,0} - \delta_z (s_x/s_z)\delta_z p_{0,0} = 0. \tag{7}$$

By expanding the finite difference operators, eq. (7) is expressed as

$$-(k^2 s_x s_z)|_{0,0} p_{0,0} \tag{8}$$

$$-\frac{1}{\Delta x^2}\left(\left(\frac{s_z}{s_x}\right)\Big|_{1/2,0}(p_{1,0}-p_{0,0})-\left(\frac{s_z}{s_x}\right)\Big|_{-1/2,0}(p_{0,0}-p_{-1,0})\right)$$
$$-\frac{1}{\Delta z^2}\left(\left(\frac{s_x}{s_z}\right)\Big|_{0,1/2}(p_{0,1}-p_{0,0})-\left(\frac{s_x}{s_z}\right)\Big|_{0,-1/2}(p_{0,0}-p_{0,-1})\right)=0.$$

Rearranging eq. (8) gives the following expression

$$\begin{aligned}&\left[-(k^2 s_x s_z)|_{0,0}+\frac{1}{\Delta x^2}\left(\left(\frac{s_z}{s_x}\right)\Big|_{1/2,0}+\left(\frac{s_z}{s_x}\right)\Big|_{-1/2,0}\right)\right.\\&\qquad\left.+\frac{1}{\Delta z^2}\left(\left(\frac{s_x}{s_z}\right)\Big|_{0,1/2}+\left(\frac{s_x}{s_z}\right)\Big|_{0,-1/2}\right)\right]p_{0,0}\\&-\frac{1}{\Delta x^2}\left(\frac{s_z}{s_x}\right)\Big|_{1/2,0}p_{1,0}-\frac{1}{\Delta x^2}\left(\frac{s_z}{s_x}\right)\Big|_{-1/2,0}p_{-1,0}\\&-\frac{1}{\Delta z^2}\left(\frac{s_x}{s_z}\right)\Big|_{0,1/2}p_{0,1}-\frac{1}{\Delta z^2}\left(\frac{s_x}{s_z}\right)\Big|_{0,-1/2}p_{0,-1}=0.\end{aligned}\tag{9}$$

Eq. (9) can be implemented practically by defining only three coefficients of $p_{0,0}$, $p_{0,1}$ and $p_{1,0}$ (depending on node ordering convention) because of the symmetry. The upper triangular part of a matrix is usually used as an input for direct sparse matrix solvers. The naïve 5-point method cannot be used in a high frequency ω or high wavenumber k region due to severe numerical dispersion, which should be reduced by dispersion-minimizing methods. However, the discretization of the symmetric PML may not yield a symmetric matrix when we incorporate a dispersion-minimizing method. We suggest a simple method to preserve the symmetry of the discretized matrix even if a dispersion-minimizing method is employed.

Dispersion-Minimizing Discretization with the Symmetric PML

In the context of exploration geophysics, most dispersion-minimizing methods (Hustedt et al., 2004; Operto et al., 2007; Chen, 2014) are based on Jo et al. (1996), which uses Marfurt's (1984) idea of mass matrix and a combination of two different spatial derivatives on the compact 9-point stencil. We also use Jo et al.'s (1996) idea to minimize the dispersion from the spatial discretization error.

Jo et al. (1996) combines conventional 5-point Laplacian with 45-degree rotated Laplacian to incorporate four additional diagonal nodal points

$$\nabla^2 p \approx a\nabla^2_{(0)}p + (1-a)\nabla^2_{(45)}p, \tag{10}$$

where $\nabla^2_{(0)}$ and $\nabla^2_{(45)}$ are discretized versions of the Laplacian. Jo et al. (1996)'s combined Laplacian has a restriction of equal grid intervals $\Delta x = \Delta z$, which can be relaxed by using the following finite difference operators

$$\begin{aligned}\delta_x^{2D} p_{0,0} &= \left(\frac{1}{2\Delta x}\right)\left(p_{\frac{1}{2},\frac{1}{2}} - p_{-\frac{1}{2},\frac{1}{2}} + p_{\frac{1}{2},-\frac{1}{2}} - p_{-\frac{1}{2},-\frac{1}{2}}\right),\\ \delta_z^{2D} p_{0,0} &= \left(\frac{1}{2\Delta z}\right)\left(p_{\frac{1}{2},\frac{1}{2}} + p_{-\frac{1}{2},\frac{1}{2}} - p_{\frac{1}{2},-\frac{1}{2}} - p_{-\frac{1}{2},-\frac{1}{2}}\right).\end{aligned} \tag{11}$$

While requiring more neighbor nodal points at staggered positions, eq. (11) has the same second order of accuracy with the finite difference operators of eq. (5). We can form a Laplacian using eq. (11) in non-PML region ($s_x = s_z = 1$) as below

$$\begin{aligned}&((\delta_x^{2D})^2 + (\delta_z^{2D})^2)p_{0,0} =\\ &\big(p_{1,1} - 2p_{0,1} + p_{-1,1} + 2p_{1,0} - 4p_{0,0} + 2p_{-1,0} + p_{1,-1} - 2p_{0,-1}\\ &\qquad + p_{-1,-1}\big)/(4\Delta x^2)\\ &+(p_{1,1} + 2p_{0,1} + p_{-1,1} - 2p_{1,0} - 4p_{0,0} - 2p_{-1,0} + p_{1,-1} + 2p_{0,-1} +\\ &\qquad p_{-1,-1})/(4\Delta z^2),\end{aligned} \tag{12}$$

which has second order of accuracy

$$(\delta_x^{2D})^2 + (\delta_z^{2D})^2 = \partial_x^2 + \partial_z^2 + O(\Delta x^2, \Delta z^2). \tag{13}$$

If $h = \Delta x = \Delta z$, then eq. (12) is simplified to

$$\begin{aligned}((\delta_x^{2D})^2 + (\delta_z^{2D})^2)p_{0,0} = (p_{1,1} + p_{1,-1} - 4p_{0,0} + p_{-1,1} + p_{-1,-1})/\\ \left(\sqrt{2}h\right)^2,\end{aligned} \tag{14}$$

which is equivalent to a Laplacian on 45-degree rotated grids as in Jo et al. (1996)'s work. Thus, eq. (12) contains eq. (14) as a special case of $\Delta x = \Delta z$. Unlike $(\delta_x^{2D})^2 + (\delta_z^{2D})^2$, the naïve finite difference $\delta_{x'}^2 + \delta_{z'}^2$ on the rotated grids (x', z') with unequal grid size $\Delta x \neq \Delta z$ actually does not give a Laplacian as follows

$$\delta_{x'}^2 + \delta_{z'}^2 = (2/(\Delta x^2 + \Delta z^2))(\Delta x^2 \partial_x^2 + \Delta z^2 \partial_z^2) + O(\Delta x^2, \Delta z^2). \tag{15}$$

Similar to eq. (10), we blend two versions of generalized Laplacian with the PML coefficients

$$\begin{aligned} &\partial_x\left(\frac{s_z}{s_x}\right)\partial_x+\partial_z\left(\frac{s_x}{s_z}\right)\partial_z \approx \\ &a\left(\delta_x\left(\frac{s_z}{s_x}\right)\delta_x+\delta_z\left(\frac{s_x}{s_z}\right)\delta_z\right) \\ &+(1-a)\left(\delta_x^{2D}\left(\frac{s_z}{s_x}\right)\delta_x^{2D}+\delta_z^{2D}\left(\frac{s_x}{s_z}\right)\delta_z^{2D}\right) \quad , \end{aligned} \tag{16}$$

which gives a symmetric discretization of the generalized Laplacian.

The averaging method is also used to replace the term $p_{0,0}$ with a combination of neighboring nodal points as follows

$$\begin{aligned} p_{0,0} \rightarrow\ & cp_{0,0}+d\left(p_{1,0}+p_{-1,0}+p_{0,1}+p_{0,-1}\right)+e(p_{1,1}+p_{1,-1}+p_{-1,1} \\ &+p_{-1,-1}) \end{aligned} \tag{17}$$

with a restriction of $c+4d+4e=1$, which means that the summation of weighting coefficients of the neghibor nodes is unity. However, if the averaging method is used as is, then it breaks the symmetry of the symmetric PML. We need to average the term $k^2 s_x s_z p$ as a whole with a caution to keep the discretization symmetric in the form of

$$(k^2 s_x s_z)|_{\frac{i}{2},\frac{j}{2}} p_{i,j}, \tag{18}$$

where $i=-1,0,1$ and $j=-1,0,1$. Then, the averaging method and the combined Laplacian [eq. (16)] are put together to form the symmetric disretization

$$\begin{aligned} &-\mathrm{c}(k^2 s_x s_z)|_{0,0} p_{0,0} \\ &-d\left((k^2 s_x s_z)|_{\frac{1}{2},0} p_{1,0}+(k^2 s_x s_z)|_{-\frac{1}{2},0} p_{-1,0}+(k^2 s_x s_z)|_{0,\frac{1}{2}} p_{0,1}\right. \\ &\qquad \left.+(k^2 s_x s_z)|_{0,-\frac{1}{2}} p_{0,-1}\right) \\ &-e\left((k^2 s_x s_z)|_{\frac{1}{2},\frac{1}{2}} p_{1,1}+(k^2 s_x s_z)|_{\frac{1}{2},-\frac{1}{2}} p_{1,-1}+(k^2 s_x s_z)|_{-\frac{1}{2},\frac{1}{2}} p_{-1,1}\right. \\ &\qquad \left.+(k^2 s_x s_z)|_{-\frac{1}{2},-\frac{1}{2}} p_{-1,-1}\right) \\ &-a\left(\delta_x\left(\frac{s_z}{s_x}\right)\delta_x+\delta_z\left(\frac{s_x}{s_z}\right)\delta_z\right)p_{0,0} \\ &\qquad -(1-a)\left(\delta_x^{2D}\left(\frac{s_z}{s_x}\right)\delta_x^{2D}+\delta_z^{2D}\left(\frac{s_x}{s_z}\right)\delta_z^{2D}\right)p_{0,0}=0. \end{aligned} \tag{19}$$

With assumptions of homogeneous medium and $s_x = s_z = 1$ and $\Delta x = \Delta z$, eq. (19) reduces to the form of Jo et al. (1996), thus we can just use weights a, c, d and e derived in Jo et al. (1996)'s work. The values of optimized coefficients are $a = 0.5461$, $c = 0.6248$, $d = 0.09381$ and $e = 1\times10^{-5}$. Because the diagonal nodal contribution e is small, we use $a = 0.5461,\ c = 0.6248,\ d = 0.0938$ and $e = 0$ for simplification of the numerical implementation.

For easy numerical implementation, eq. (19) can be expanded and rearranged to

$$
\begin{aligned}
&\left[-\mathrm{c}(k^2 s_x s_z)|_{0,0} + \frac{a}{\Delta x^2}\left(\frac{s_z}{s_x}\Big|_{\frac{1}{2},0} + \frac{s_z}{s_x}\Big|_{-\frac{1}{2},0}\right) + \frac{a}{\Delta z^2}\left(\frac{s_x}{s_z}\Big|_{0,\frac{1}{2}} + \frac{s_x}{s_z}\Big|_{0,-\frac{1}{2}}\right)\right.\\
&\qquad + \frac{1-a}{4\Delta x^2}\left(\frac{s_z}{s_x}\Big|_{\frac{1}{2},\frac{1}{2}} + \frac{s_z}{s_x}\Big|_{-\frac{1}{2},\frac{1}{2}} + \frac{s_z}{s_x}\Big|_{\frac{1}{2},-\frac{1}{2}} + \frac{s_z}{s_x}\Big|_{-\frac{1}{2},-\frac{1}{2}}\right)\\
&\qquad \left. + \frac{1-a}{4\Delta z^2}\left(\frac{s_x}{s_z}\Big|_{\frac{1}{2},\frac{1}{2}} + \frac{s_x}{s_z}\Big|_{-\frac{1}{2},\frac{1}{2}} + \frac{s_x}{s_z}\Big|_{\frac{1}{2},-\frac{1}{2}} + \frac{s_x}{s_z}\Big|_{-\frac{1}{2},-\frac{1}{2}}\right)\right] p_{0,0}\\
&+\left[-d(k^2 s_x s_z)|_{0,\frac{1}{2}} - \frac{a}{\Delta z^2}\frac{s_x}{s_z}\Big|_{0,\frac{1}{2}} + \frac{1-a}{4\Delta x^2}\left(\frac{s_z}{s_x}\Big|_{\frac{1}{2},\frac{1}{2}} + \frac{s_z}{s_x}\Big|_{-\frac{1}{2},\frac{1}{2}}\right)\right.\\
&\qquad \left. - \frac{1-a}{4\Delta z^2}\left(\frac{s_x}{s_z}\Big|_{\frac{1}{2},\frac{1}{2}} + \frac{s_x}{s_z}\Big|_{-\frac{1}{2},\frac{1}{2}}\right)\right] p_{0,1}\\
&-\left[\frac{1-a}{4\Delta x^2}\frac{s_z}{s_x}\Big|_{\frac{1}{2},-\frac{1}{2}} + \frac{1-a}{4\Delta z^2}\frac{s_x}{s_z}\Big|_{\frac{1}{2},-\frac{1}{2}}\right] p_{1,-1}\\
&+\left[-d(k^2 s_x s_z)|_{\frac{1}{2},0} - \frac{a}{\Delta x^2}\frac{s_z}{s_x}\Big|_{\frac{1}{2},0} - \frac{1-a}{4\Delta x^2}\left(\frac{s_z}{s_x}\Big|_{\frac{1}{2},\frac{1}{2}} + \frac{s_z}{s_x}\Big|_{\frac{1}{2},-\frac{1}{2}}\right)\right.\\
&\qquad \left. + \frac{1-a}{4\Delta z^2}\left(\frac{s_x}{s_z}\Big|_{\frac{1}{2},\frac{1}{2}} + \frac{s_x}{s_z}\Big|_{\frac{1}{2},-\frac{1}{2}}\right)\right] p_{1,0}\\
&-\left[\frac{1-a}{4\Delta x^2}\frac{s_z}{s_x}\Big|_{\frac{1}{2},\frac{1}{2}} + \frac{1-a}{4\Delta z^2}\frac{s_x}{s_z}\Big|_{\frac{1}{2},\frac{1}{2}}\right] p_{1,1}\\
&\qquad +\text{the other terms for } p_{-1,-1}, p_{-1,0}, p_{-1,1}, p_{0,-1} = 0.
\end{aligned}
\tag{20}
$$

Eq. (20) can be implemented directly into codes by assigning only 5 coefficients of $p_{0,0}$, $p_{0,1}$, $p_{1,-1}$, $p_{1,0}$ and $p_{1,1}$, not whole 9 coefficients because of the symmetry.

Dispersion Analysis

Numerical dispersion characteristic of the symmetric PML equation is equivalent to that of Jo et al. (1996)'s work, when $\Delta x = \Delta z$. If the grid interval Δx and Δz are not the same, then the dispersion characteristic may not be optimal with the weighting parameters given in Jo et al. (1996). To analyze the effect of aspect ratio of grid intervals, we assume that the PML coefficients s_x, s_z are unity and the medium is homogeneous (a constant velocity value). Then eq. (19) with the weighting parameter $e = 0$ becomes

$$\begin{aligned} &-k^2\left(cp_{0,0} + d\left(p_{1,0} + p_{-1,0} + p_{0,1} + p_{0,-1}\right)\right) \\ &-a\left(\delta_x^2 p_{0,0} + \delta_z^2 p_{0,0}\right) \\ &-(1-a)\left((\delta_x^{2D})^2 p_{0,0} + (\delta_x^{2D})^2 p_{0,0}\right) = 0 \ . \end{aligned} \tag{21}$$

The relation between a true wavenumber k and a numerical wavenumber k_{num} can be computed by inserting an ansatz solution such as $p_{0,0} = \exp(i(k_x x + k_z z))$ and $p_{1,0} = \exp(i(k_x(x + \Delta x) + k_z z))$ with $k_x = k_{\text{num}} \cos(\theta)$ and $k_z = k_{\text{num}} \sin(\theta)$, where θ is a propagation angle (from the x-axis) of a plane wave. If we express the finite difference operators as a pseudo differential operator form like $\delta_x = 2\sinh(\Delta x \partial_x/2)\,/\,\Delta x$, the finite difference operators in eq. (21) can be easily replaced with the corresponding spatially Fourier-transformed expressions, for example, $\delta_x \rightarrow 2i\sin(k_x \Delta x/2)\,/\Delta x$ as follows

$$\begin{aligned} &-k^2\left(c + 2d(\cos(k_x\Delta x) + \cos(k_z\Delta z))\right) \\ &+a\left(\frac{4}{\Delta x^2}\sin^2\left(\frac{k_x\Delta x}{2}\right) + \frac{4}{\Delta z^2}\sin^2\left(\frac{k_z\Delta z}{2}\right)\right) \\ &+\frac{(1-a)}{\Delta x^2}\left(\sin\left(\frac{k_x\Delta x - k_z\Delta z}{2}\right) + \sin\left(\frac{k_x\Delta x + k_z\Delta z}{2}\right)\right)^2 \\ &+\frac{(1-a)}{\Delta z^2}\left(\sin\left(\frac{-k_x\Delta x + k_z\Delta z}{2}\right) + \sin\left(\frac{k_x\Delta x + k_z\Delta z}{2}\right)\right)^2 = 0 \ . \end{aligned} \tag{22}$$

From eq. (22), we can compute a ratio of wavenumbers [or equivalently, a ratio of velocities as in Marfurt (1984); Jo et al. (1996)] $v_{\text{num}}/v = k/k_{\text{num}}$, which is a function of $k_{\text{num}} \max(\Delta x, \Delta z) = 2\pi/G$, where G is the number of grid points per wavelength in the direction of the largest grid interval. $1/G$ should be defined by the largest grid interval $\max(\Delta x, \Delta z)$ to properly plot dispersion curves in the $1/G$ range from 0 to 0.25.

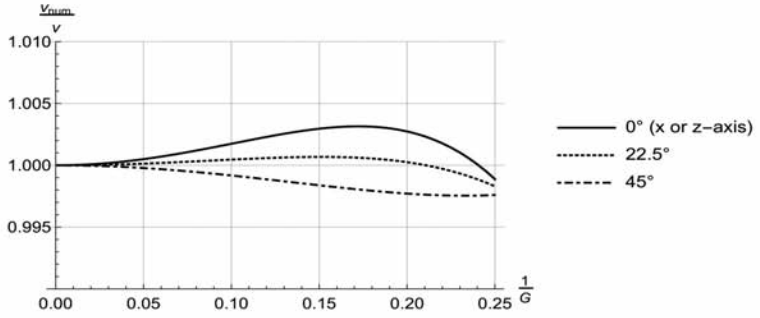

(a) $\Delta z = \Delta x$. The curves are the same with those of Jo et al. (1996).

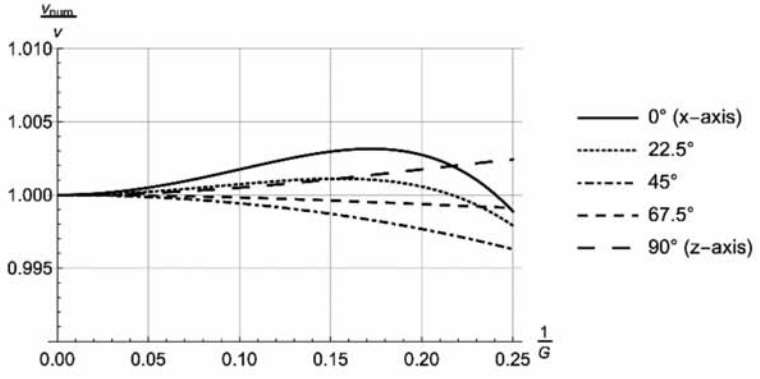

(b) $\Delta z = 0.5\Delta x$

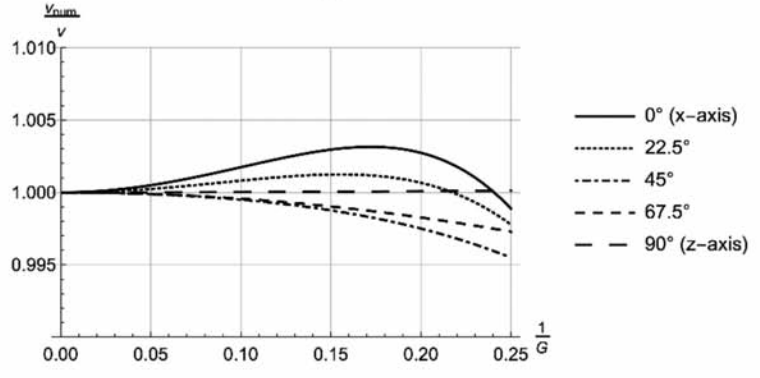

(c) $\Delta z = 0.1\Delta x$

Fig. 1. Normalized phase velocity. Closer to 1 is better. Fig. 1(a) shows that there are slight phase lead and lag depending on the propagation direction but the error is bounded within 0.5 percent in the plot range ($1/G < 0.25$). Figs. 1(b) and 1(c) show that the unequal grid size is not helpful for improving the dispersion characteristic because of the dominant error in the direction of the largest grid interval (Δx in this case).

Fig. 1 shows the improved dispersion curves along some propagation angles and aspect ratios of grid intervals, compared to the naïve second order finite difference method [eq. (7)], which always has the phase lag ($v_{\text{num}}/v < 1$) in every direction (see Jo et al., 1996). The error of the normalized phase velocity is less than 0.5% for all aspect ratios with $1/G < 0.25$. Thus, we may use various unequal grid intervals simply with the optimized parameters a, c and d that is computed when $\Delta x = \Delta z$. Of course, the weighting parameters can be further optimized for each aspect ratio as in Chen (2013), although the parameters do not vary significantly along different aspect ratios.

Despite the flexibility of aspect ratio, there may be a reason not to use unequal grid intervals $\Delta x \neq \Delta z$. In Fig. 1(c), even if the grid interval in the z direction ($\theta = 90°$) decreases by a factor of 10 relative to Δx, the error in the x direction ($\theta = 0°$) does not decrease at all. In this situation, the dominant error comes from the direction with the largest grid interval, so it invalidates the error reduction of the smaller grid interval.

EXAMPLES

Computational Costs

A numerical experiment was conducted on a single 8-CPU node using Parallel Direct Sparse Solver for Clusters included in Intel Math Kernel Library (Kalinkin et al., 2014), which incorporates METIS (Karypis and Kumar, 1998) as a fill-in reducing reordering method. If we consider a 2D elliptic boundary value problem on a regular $n \times n$ square mesh, METIS and nested dissection ordering algorithms give the storage complexity $O(n^2 \log(n))$ and arithmetic operations $O(n^3)$ for sparse matrix factorization (George, 1973). We solved a 2D Helmholtz problem in a $n \times n$ grid. Four boundaries are set to the PML and a point source was located at the center of the computational domain. Because the reordering process is dependent only on the matrix connectivity, so it can be done independently with the frequency and boundary conditions if the matrix connectivity remains the same. Although symmetric and nonsymmetric cases have the same form of computational complexity, symmetric one reduces the storage requirement (54%) and arithmetic operations (57%) (Fig. 2), when we compute ratios of asymptotic expressions $O(n^2 \log(n))$ and $O(n^3)$, respectively. Computational time in Fig. 3 was obtained from averaging 10 numerical experiments and it shows that the LDLT decomposition using a symmetric matrix is more efficient than the LU decomposition also in terms of computational time.

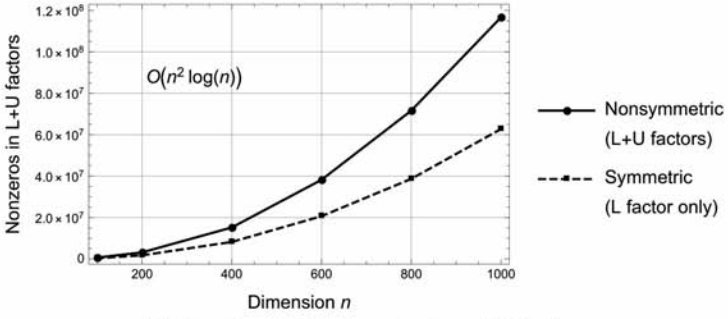

(a) Numbers of nonzero in L and U factors

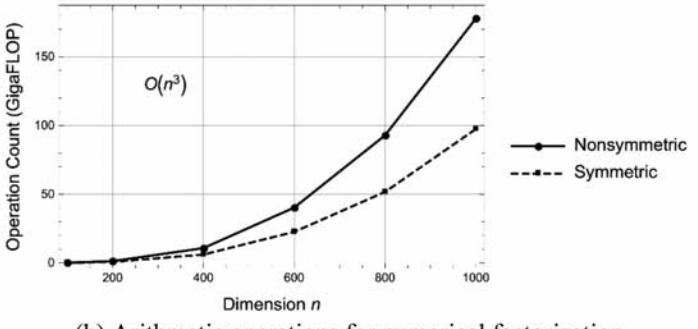

(b) Arithmetic operations for numerical factorization

Fig. 2. Computational complexities from a 2D Helmholtz problem in square $n \times n$ grids. Lower is better. Fig. 2(a) shows the reduced memory usage of a symmetric matrix (about 54% of nonsymmetric one). Fig. 2(b) shows the reduced arithmetic operations (about 57% of nonsymmetric one).

Comparison with the Analytic Solution

The analytic solutions for the unit impulse source with various frequencies were computed from the Hankel function expression (If $\mathrm{Im}(k) > 0$, then $iH_0^{(1)}(kr)/4$. If $\mathrm{Im}(k) < 0$, then $-iH_0^{(2)}(kr)/4$) and the corresponding numerical solutions were computed from the symmetric discretization [eq. (20)] with the domain size of 5 km $\times$ 5 km and the grid interval $\Delta x = \Delta z = 0.025$ km. Representatively, time-harmonic wavefields at two specific frequencies are presented in Fig. 4, where both numerical solutions are matched well with the analytic solutions.

We also synthesized a time domain seismogram with a source wavelet. Time-harmonic solutions were computed at each frequency in the range of 0-15 Hz with a frequency interval $1/T_{\max}$, where $T_{\max} = 10$ s is a maximum recording time. Each spatial grid interval is 0.025 km. The size of the computational domain was extended to cover up to 10 km offset. The source wavelet function is a Ricker wavelet with the peak frequency of 5 Hz, whose

frequency spectrum contains up to about 15 Hz. We transformed the frequency domain solutions to the time domain (Fig. 5) by the discrete Fourier transform. In Fig. 5, analytic and numerical traces are matched quite well.

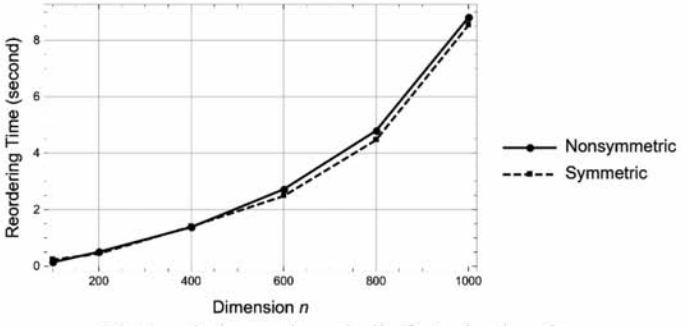

(a) Reordering and symbolic factorization time

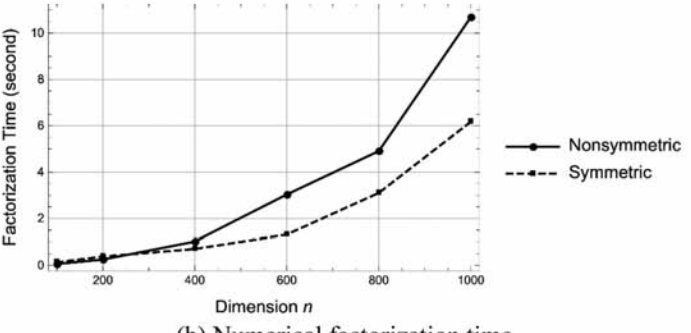

(b) Numerical factorization time

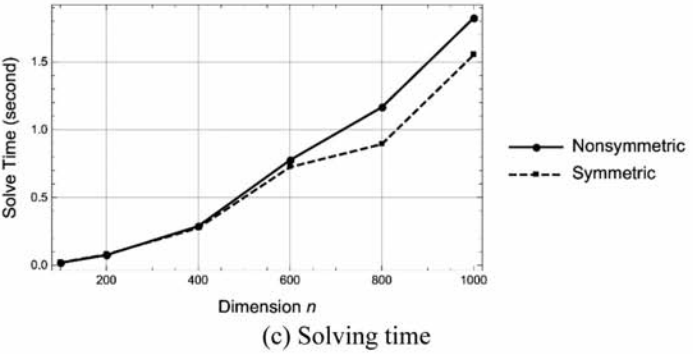

(c) Solving time

Fig. 3. Timing from a 2D Helmholtz problem in square $n \times n$ grids. Lower is better. Timing was conducted by averaging 10 individual experiments. The curves of Fig. 3(b) approximately follow the complexity of Fig. 2(b), although the ratio of time is not regular along the dimension n. Reordering and solving efficiencies are improved slightly, however they may depend on implementation of sparse matrix solvers. The slight efficiency gain might come from reduction of memory access and allocation.

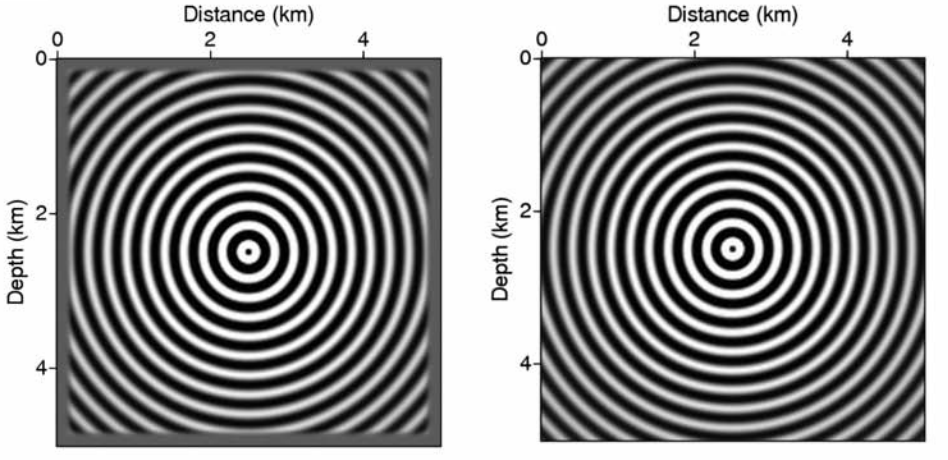

(a) Modeled wavefield at $1/G = 0.1$ corresponding to 6 Hz

(b) Analytic wavefield corresponding to the wavenumber of Fig. 4(a)

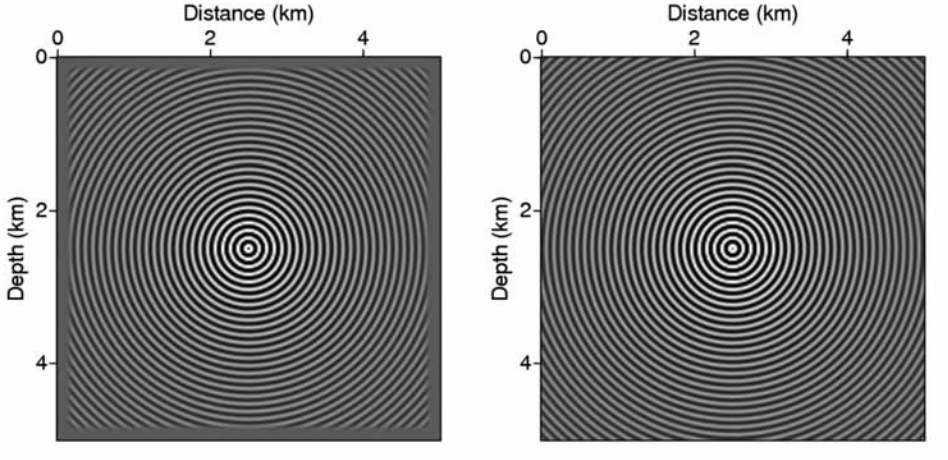

(c) Modeled wavefield at $1/G = 0.25$ corresponding to 15 Hz

(d) Analytic wavefield corresponding to the wavenumber of Fig. 4(c)

Fig. 4. Wavefields from a homogeneous medium (1.5 km/s) in a 5 $\times$ 5 km domain with the grid interval of 0.025 km. The point source is located at the center of the domain. In contrast to the analytic solutions [Figs. 4(b) and 4(d)], there are decaying wavefields near the boundaries in the numerical solutions [Figs. 4(a) and 4(c)] because of the PML. From the moderate frequency ($1/G = 0.1$) to the high frequency ($1/G = 0.25$), the numerical solutions are matched well with the analytic solutions.

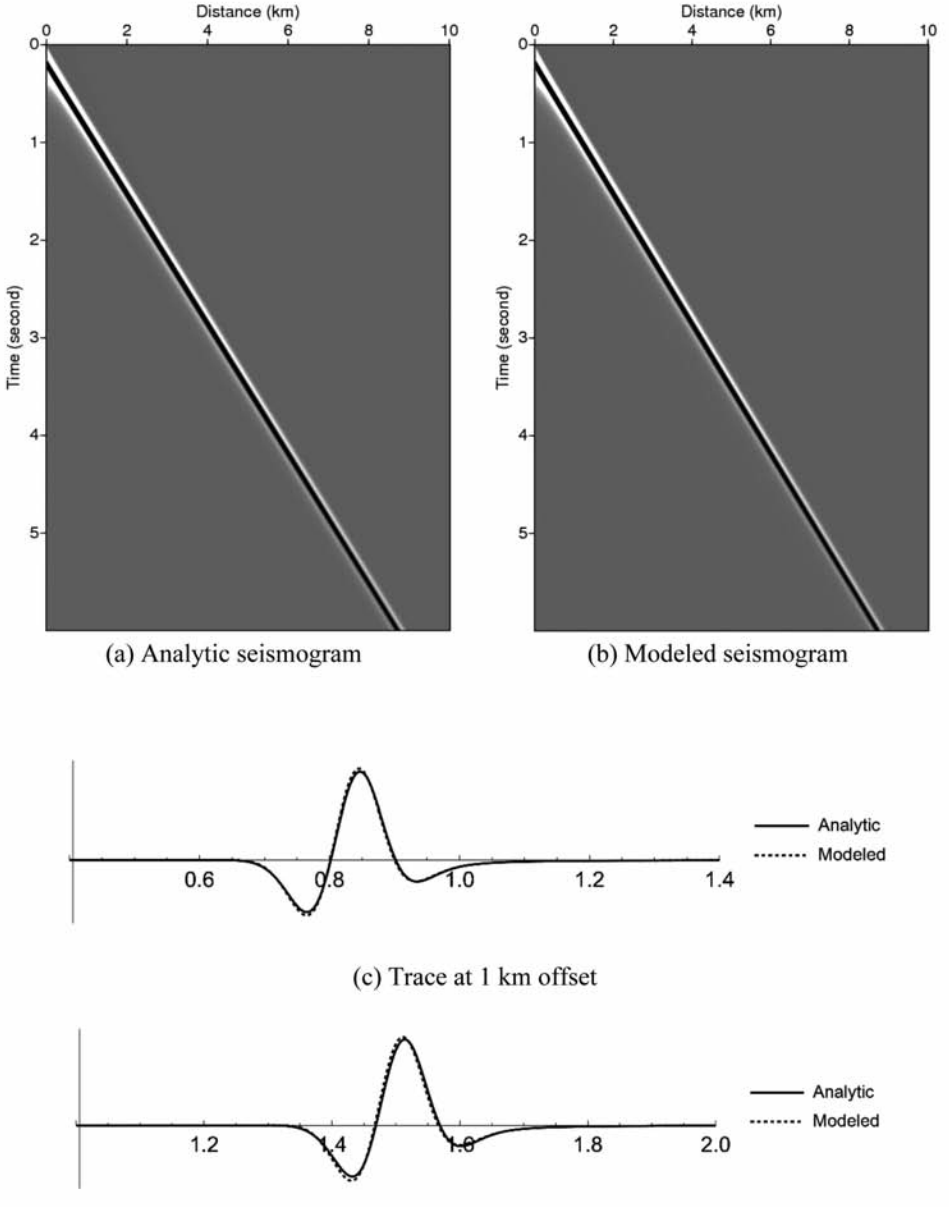

(a) Analytic seismogram

(b) Modeled seismogram

(c) Trace at 1 km offset

(d) Trace at 2 km offset

Fig. 5. Comparison between analytic and modeled seismograms using a Ricker wavelet with the peak frequency of 5 Hz (the maximum frequency is about 15 Hz) in a homogeneous medium (1.5 km/s). The analytic and numerical solutions match well.

Heterogeneous Velocity Model

The symmetric discretization was applied to the heterogeneous velocity model called SEG/EAGE 3D salt (Aminzadeh et al., 1997). Except the velocity model and the free surface boundary condition on the top of the model, the rest of conditions are the same with the previous experiment of analytic solution. Left, right and bottom boundaries are set to the PML. Grid intervals $\Delta x = \Delta z$ are 0.025 km the grid dimension (n_x, n_z) is $(623, 167)$. And a Ricker wavelet is used with the peak frequency of 5 Hz, and its frequency spectrum contains up to about 15 Hz. We generated wavefields at frequency 5 Hz [Fig. 6(b)] and 15 Hz [Fig. 6(c)] from a smoothed velocity model of the original salt model [Fig. 6(a)] to avoid the staircase effect. Seismograms [Figs. 7(a) and 7(b)] were also synthesized from the frequency domain modeling with the nonsymmetric and symmetric discretization. The results from both symmetric and nonsymmetric methods are qualitatively the same. Although there is a slight amplitude difference in the PML region, especially at 0 km distance, Fig. 7(c) shows there is no considerable difference in the main computational domain. Table 1 shows the comparison of the computational costs between the nonsymmetric and symmetric cases for this test. Thus, we can tell the proposed symmetric discretization reduces the computational costs significantly.

Table 1. Comparison of the computational costs for each frequency with the SEG/EAGE salt model of the grid dimension $(n_x, n_z) = (623,167)$. Arithmetic count and the number of nonzeros are reduced by half, however the ratio of the factorization time is somewhat larger than the ratio of the others. There may be an overhead in the actual factorization procedure of the direct sparse matrix solver.

	Symmetric	Nonsymmetric	Ratio
Arithmetic count (GigaFlop)	3.075215	5.383508	57.12%
The number of nonzeros	5004409	9241281	54.15%
Factorization time (second)	0.246417	0.363739	67.75%

CONCLUSIONS

A symmetrization procedure of the dispersion-minimizing method with the PML for the Helmholtz equation was introduced. With the symmetric formulation, the computational costs are reduced by half in terms of the arithmetic count and memory requirement. To our best knowledge, the symmetric form of the PML has not been widely used in the exploration geophysics communities. Although we showed only 2D problems, which are

not costly with the current computing power, the suggested scheme would be more beneficial to applications such as 3D full waveform inversion and reverse time migration in the frequency domain. The proposed approach will be applied to the 3D Helmholtz equation in the near future.

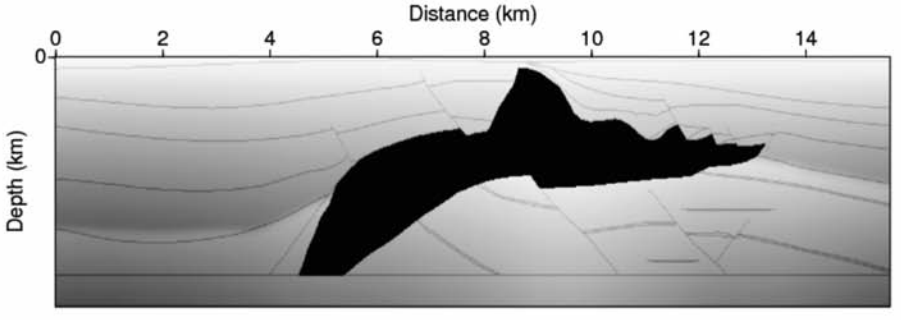

(a) P-wave velocity model

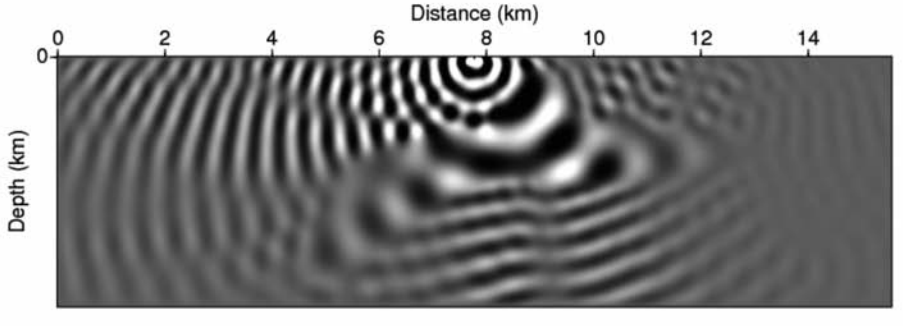

(b) Real part of a complex-valued wavefield at 5Hz

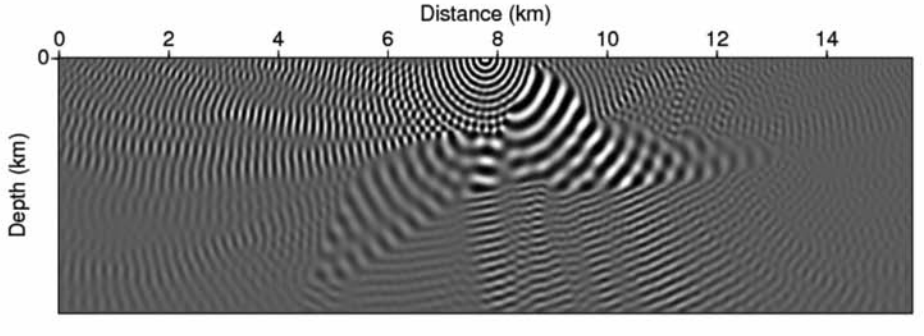

(c) Real part of a complex-valued wavefield at 15 Hz

Fig. 6. The SEG/EAGE salt velocity model and wavefields with grid size of 0.025 km.

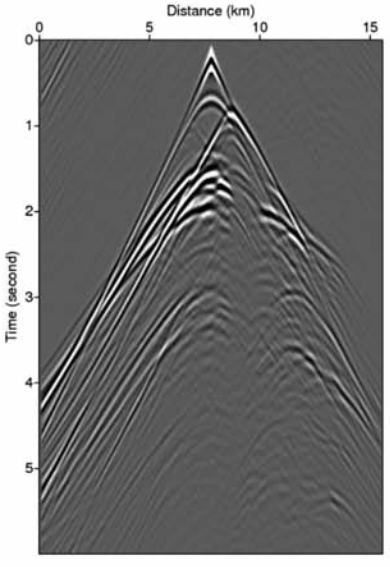

(a) Seismogram from the nonsymmetric discretization

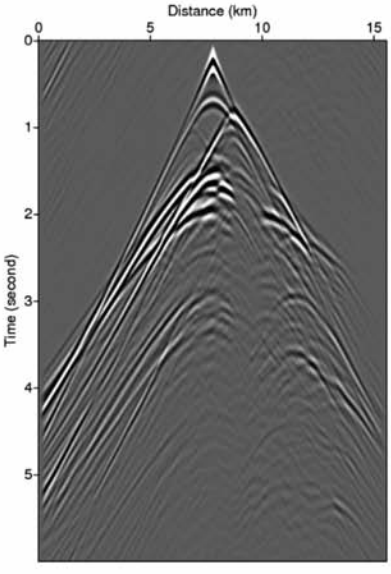

(b) Seismogram from the symmetric discretization

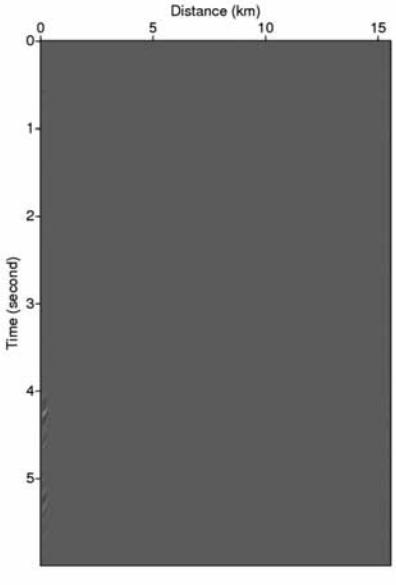

(c) Difference between 7(a) and 7(b)

Fig. 7. Seismograms from both nonsymmetric and symmetric cases. The difference plot 7(c) in the same scale of 7(a) and 7(b) shows that there is no noticeable difference except the PML domain at 0 km distance. Note that some signals appear before the direct arrivals, because the wraparound effect was caused by the discrete Fourier transform with the finite frequency interval $1/T_{\max}$. If $T_{\max}$ gets large enough, then the wraparound effect will disappear, but it needs more computation.

ACKNOWLEDGMENTS

This work was supported by the Energy Efficiency & Resources Core Technology Program of the Korea Institute of Energy Technology Evaluation and Planning (KETEP), granted financial resource from the Ministry of Trade, Industry & Energy, Republic of Korea (Nos. 20132510100060 and 20152520100740). The Institute of Engineering Research at Seoul National University provided research facilities for this work.

REFERENCES

Aminzadeh, F., Brac, J. and Kunz, T., 1997. 3D Salt and Overthrust Model. Modeling Series i, SEG, Tulsa, OK.

Baysal, E., Kosloff, D.D. and Sherwood, J.W.C., 1983. Reverse time migration. Geophysics, 48: 1514-1524.

Bérenger, J.-P., 1994. A perfectly matched layer for the absorption of electromagnetic waves: J. Computat. Phys., 114: 185-200.

Bérenger, J.-P., 2007. Perfectly matched layer (pml) for computational electromagnetics. Synthesis Lectures on Computat. Electromagnet., 2: 1-117.

Bunch, J.R., and Kaufman, L., 1977. Some stable methods for calculating inertia and solving symmetric linear systems. Mathemat. Computat., 31: 163-179.

Chen, J.-B., 2013. A generalized optimal 9-point scheme for frequency-domain scalar wave equation. J. Appl. Geophys., 92: 1-7.

Chen, J.-B., 2014. A 27-point scheme for a 3D frequency-domain scalar wave equation based on an average-derivative method. Geophys. Prosp., 62: 258-277.

Chew, W.C. and Weedon, W.H., 1994. A 3D perfectly matched medium from modified Maxwell's equations with stretched coordinates. Microwave Optic. Technol. Lett., 7: 599-604.

George, A., 1973,. Nested dissection of a regular finite element mesh. SIAM J. Numer. Analys., 10: 345-363.

Hustedt, B., Operto, S. and Virieux, J., 2004. Mixed-grid and staggered-grid finite-difference methods for frequency-domain acoustic wave modeling. Geophys. J. Internat., 157: 1269-1296.

Jo, C., Shin, C. and Suh, J., 1996. An optimal 9-point, finite-difference, frequency- space, 2-D scalar wave extrapolator. Geophysics, 61: 529-537.

Kalinkin, A., Anders, A. and Anders, R., 2014. Intel math Kernel library parallel direct sparse olver for clusters. EAGE Workshop on High Performance Computing for Upstream, Chania, Crete, Greece.

Karypis, G. and Kumar, V., 1998. A fast and high quality multilevel scheme for partitioning irregular graphs. SIAM J. Scientif. Comput., 20: 359-392.

Marfurt, K., 1984. Accuracy of finite-difference and finite-element modeling of the scalar and elastic wave equations. Geophysics, 49: 533-549.

Operto, S., Virieux, J., Amestoy, P., L'Excellent, J.-Y., Giraud, L. and Ali, H.B.H., 2007. 3D finite-difference frequency-domain modeling of visco-acoustic wave propagation using a massively parallel direct solver: A feasibility study. Geophysics, 72(5): SM195-SM211.

Pratt, R.G., Shin, C. and Hick, G., 1998 Gauss-Newton and full Newton methods in frequency-space seismic waveform inversion. Geophys. J. Internat., 133: 341-362.

Sacks, Z., Kingsland, D., Lee, R. and Lee, J.-F., 1995. A perfectly matched anisotropic absorber for use as an absorbing boundary condition. IEEE Transact. Antenn. Propagat., 43: 1460-1463.

Shin, C., 1988. Nonlinear Elastic Wave Inversion by Blocky Parameterization. Ph.D. thesis, University of Tulsa, OK.

Tarantola, A., 1984. Inversion of seismic reflection data in the acoustic approximation. Geophysics, 49: 1259-1266.

Turkel, E. and Yefet, A., 1998. Absorbing PML boundary layers for wave-like equations. Appl. Numer. Mathemat., 27:533-557.